




# Furosemide rescues hypercalciuria in familial hypomagnesaemia with hypercalciuria and nephrocalcinosis model

Natalia Kriuchkova<sup>1</sup>  | Tilman Breiderhoff<sup>2</sup> | Dominik Müller<sup>2</sup> |  
Duygu Elif Yilmaz<sup>3</sup> | Hasan Demirci<sup>3</sup> | Hoora Drewell<sup>1</sup> | Dorothee Günzel<sup>4</sup> |  
Nina Himmerkus<sup>5</sup> | Markus Bleich<sup>5</sup>  | Pontus B. Persson<sup>1</sup> | Kerim Mutig<sup>1</sup> 

<sup>1</sup>Department of Translational Physiology, Charité-Universitätsmedizin Berlin, Berlin, Germany

<sup>2</sup>Division of Gastroenterology, Nephrology and Metabolic Diseases, Department of Pediatrics, Charité-Universitätsmedizin Berlin, Berlin, Germany

<sup>3</sup>Department of Functional Anatomy, Charité-Universitätsmedizin Berlin, Berlin, Germany

<sup>4</sup>Clinical Physiology/Division of Nutritional Medicine, Charité-Universitätsmedizin Berlin, Berlin, Germany

<sup>5</sup>Institute of Physiology, Kiel University, Kiel, Germany

## Correspondence

Kerim Mutig, Department of Translational Physiology, Charité-Universitätsmedizin Berlin, Virchowweg 6, Berlin 10117, Germany.  
Email: [kerim.mutig@charite.de](mailto:kerim.mutig@charite.de)

## Funding information

Deutsche Forschungsgemeinschaft, Grant/Award Number: Project ID 394046635 - SFB 1365

## Abstract

**Aim:** Perturbed calcium homeostasis limits life expectancy in familial hypomagnesaemia with hypercalciuria and nephrocalcinosis (FHHNC). This rare disease occurs by loss-of-function mutations in CLDN16 or CLDN19 genes, causing impaired paracellular reabsorption of divalent cations along the cortical thick ascending limb (cTAL). Only partial compensation takes place in the ensuing late distal convoluted tubule, connecting tubule, and collecting duct, where the luminal transient receptor potential channel V5 (TRPV5), as well as basolateral plasma membrane calcium ATPase (PMCA) and sodium-potassium exchanger (NCX1) mediate transcellular  $\text{Ca}^{2+}$  reabsorption. The loop diuretic furosemide induces compensatory activation in these distal segments. Normally, furosemide enhances urinary calcium excretion via inhibition of the aforementioned cTAL. As  $\text{Ca}^{2+}$  reabsorption in the cTAL is already severely impaired in FHHNC patients, furosemide may alleviate hypercalciuria in this disease by activation of the distal transcellular  $\text{Ca}^{2+}$  transport proteins.

**Methods:** Cldn16-deficient mice (Cldn16<sup>-/-</sup>) served as a FHHNC model. Wild-type (WT) and Cldn16<sup>-/-</sup> mice were treated with furosemide (7 days of 40 mg/kg bw) or vehicle. We assessed renal electrolyte handling (metabolic cages) and key divalent transport proteins.

**Results:** Cldn16<sup>-/-</sup> mice show higher  $\text{Ca}^{2+}$  excretion than WT and compensatory stimulation of Cldn2, TRPV5, and NCX1 at baseline. Furosemide reduced hypercalciuria in Cldn16<sup>-/-</sup> mice and enhanced TRPV5 and PMCA levels in Cldn16<sup>-/-</sup> but not in WT mice.

**Conclusions:** Furosemide significantly reduces hypercalciuria, likely via upregulation of luminal and basolateral  $\text{Ca}^{2+}$  transport systems in the distal nephron and collecting duct in this model for FHHNC.

See related editorial: Wagner CA, 2023. Smart kidneys: Enhance intratubular communication to overcome disease. *Acta Physiol.* (Oxf). e13930.

This is an open access article under the terms of the [Creative Commons Attribution](https://creativecommons.org/licenses/by/4.0/) License, which permits use, distribution and reproduction in any medium, provided the original work is properly cited.

© 2023 The Authors. *Acta Physiologica* published by John Wiley & Sons Ltd on behalf of Scandinavian Physiological Society.

## KEYWORDS

claudin-16, distal calcium reabsorption, TRPV5

## 1 | INTRODUCTION

Maintenance of extracellular  $\text{Ca}^{2+}$  and  $\text{Mg}^{2+}$  levels within their narrow physiologic ranges is critical to neuronal excitability, muscle contraction, blood coagulation, bone formation, hormone secretion, and more. Inactivating mutations in genes encoding claudin-16 (Cldn16) or Cldn19 cause Familial Hypomagnesemia with Hypercalciuria and Nephrocalcinosis (FHHNC).<sup>1,2</sup> Accordingly, knockdown or knockout of Cldn16 in mice lead to pronounced urinary  $\text{Ca}^{2+}$  and  $\text{Mg}^{2+}$  wasting, thus recapitulating the human FHHNC syndrome.<sup>3,4</sup> Knockdown of Cldn19 has been shown to strongly reduce the Cldn16 abundance in the tight junctions resulting in an FHHNC-like phenotype as well.<sup>5</sup>

No specific FHHNC treatment is available; patients develop nephrocalcinosis and chronic kidney disease (CKD). Efficient therapeutic strategies providing significant improvement of life quality and retarding progression to CKD are missing.<sup>6</sup> FHHNC patients typically receive supporting therapy based on dietary magnesium supplementation to maintain adequate serum  $\text{Mg}^{2+}$  levels, as well as thiazide diuretics to reduce hypercalciuria and nephrocalcinosis.<sup>6,7</sup> However, these approaches are insufficient and the end-stage renal failure in FHHNC patients may develop making kidney transplantation mandatory.<sup>6,7</sup>

Renal handling of divalent cations encompasses several transport mechanisms mediating their transcellular or paracellular reabsorption along the proximal and distal nephron segments. The proximal tubule (PT) reabsorbs two-thirds of filtered  $\text{Ca}^{2+}$  by a paracellular route involving claudin-2 (Cldn2).<sup>8</sup> The distal nephron contributes to renal calcium handling by paracellular reabsorption along the cortical (c) thick ascending limb (cTAL) and by transcellular reabsorption in the distal convoluted tubule (DCT), connecting tubule (CNT), and collecting duct (CD).<sup>9</sup> Paracellular  $\text{Ca}^{2+}$  reabsorption in cTAL depends on functional interactions between Cldn14, Cldn16, and Cldn19.<sup>10–12</sup> Cldn16 and Cldn19 build functional heterodimers mediating divalent cation reabsorption, whereas Cldn14 inhibits this complex thus increasing urinary  $\text{Ca}^{2+}$  and  $\text{Mg}^{2+}$  excretion.<sup>12</sup> The ensuing transcellular  $\text{Ca}^{2+}$  transport along the late DCT, CNT, and, to a lesser extent, CD involves the luminal transient receptor potential cation channel subfamily V members 5 and 6 (TRPV5/6), intracellular buffering by calbindin D-28K (Calb), and basolateral exit via the plasma membrane  $\text{Ca}^{2+}$ -ATPases (PMCA; likely PMCA4) and the sodium-calcium exchanger (NCX1).<sup>9,13–15</sup>

In contrast to  $\text{Ca}^{2+}$ , the distal nephron plays the dominant role in renal magnesium handling.<sup>16,17</sup> Only 10–20% of filtered  $\text{Mg}^{2+}$  is reabsorbed in PT, whereas up to 60% of filtered  $\text{Mg}^{2+}$  is taken up in cTAL via paracellular pores formed by synergistic interactions between Cldn16 and Cldn19.<sup>10,16,17</sup> The DCT fine-tunes  $\text{Mg}^{2+}$  reabsorption via the transient receptor potential melastatin 6 (TRPM6).<sup>17</sup> Thus, the cTAL reabsorbs a major portion of filtered divalent cations via the paracellular route.

This process is functionally coupled to the transcellular NaCl transport mediated by the kidney  $\text{Na}^+$ - $\text{K}^+$ -2 $\text{Cl}^-$  cotransporter (NKCC2) and luminal  $\text{K}^+$  recycling via the renal outer medullary channel (ROMK).<sup>18</sup> The resulting lumen-positive electrical potential drives paracellular cation reabsorption along the TAL. There, Cldn16/19 complexes in the tight junctions reabsorb  $\text{Ca}^{2+}$  and  $\text{Mg}^{2+}$ .<sup>19</sup>

In the Cldn16-deficient mouse FHHNC model, severe urinary loss of  $\text{Ca}^{2+}$  and  $\text{Mg}^{2+}$  is nearly completely corrected by concomitant deletion of Cldn10b.<sup>20</sup> Cldn10b-deletion impairs paracellular  $\text{Na}^+$  reabsorption in TAL, which may induce compensatory stimulation of DCT and CNT functions including the transcellular reabsorption of divalent cations.<sup>20</sup> Loop diuretics may mimic Cldn10-deletion, as both impair sodium reabsorption in TAL.

The current management of FHHNC by thiazides falls short of markedly improving renal  $\text{Ca}^{2+}$  handling.<sup>6,7</sup> Using loop diuretics appears more intuitive than thiazides since the former exerts stronger effects. Thus, we test pharmacological inhibition of sodium reabsorption in TAL to treat Cldn16-deficiency. Using Cldn16-deficient (Cldn16<sup>-/-</sup>) mice as a model for FHHNC we demonstrate that furosemide significantly improves the calcium handling in these mice, which bears therapeutic potential for use of loop diuretics in FHHNC patients.

## 2 | RESULTS

## 2.1 | Effects of furosemide on renal electrolyte handling in WT versus Cldn16-deficient mice

To verify the genotype of Cldn16-deficient mice we performed double-labeling for Cldn16 and a tight junction (TJ)-resident protein occludin in wild-type (WT) versus Cldn16<sup>-/-</sup> kidney sections using immunofluorescence. WT kidneys exhibited overlapping Cldn16 and occludin signals in TJs of cortical but not medullary TAL cells

(Figure 1A–F,J,K). In contrast, no Cldn16 signal was detected in Cldn16<sup>-/-</sup> kidney sections (Figure 1G–I). To test the effects of the chronic furosemide application on the renal function in Cldn16-deficiency, WT

and Cldn16<sup>-/-</sup> mice were treated with daily injections of furosemide (40 mg/kg body weight, i.p.) for 7 days. Analysis of urine samples obtained in metabolic cages on the last day of experiment revealed similar 24 h urine

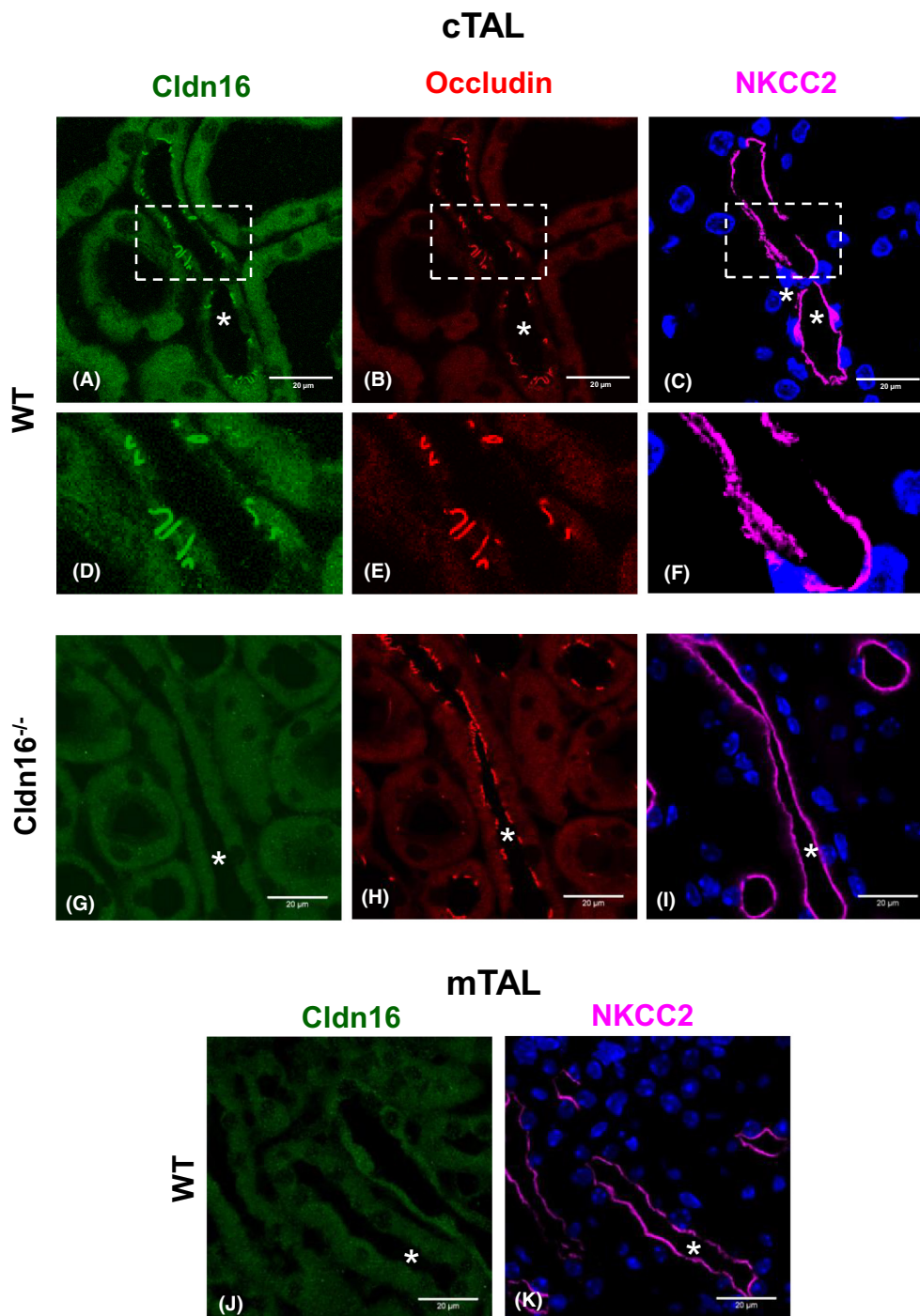


**FIGURE 1** Verification of claudin-16 (Cldn16)-deficiency in Cldn16-knockout (Cldn16<sup>-/-</sup>) mice. (A–I) Representative confocal microscopic images of cortical thick ascending limb (cTAL, \*) in wild-type (WT; A–F) or Cldn16<sup>-/-</sup> mouse kidney (G–I) triple-labeled for Cldn16 (green signal), occludin (red signal), and the thick ascending limb (TAL)-specific Na<sup>+</sup>-K<sup>+</sup>-2Cl<sup>-</sup> cotransporter (NKCC2, magenda signal). Dashed-lined inserts in A–C reflect regions presented at higher magnification in D–F. Dotted Cldn16 signal reflecting occludin signal pattern was detected in WT (A, B, D, E) but not Cldn16<sup>-/-</sup> cTAL (G,H). (J,K) Representative confocal images of WT kidney showing medullary TAL (mTAL, \*) double-labeled for Cldn16 and NKCC2, note the absence of Cldn16 signal in mTAL; N = 3 for WT and Cldn16<sup>-/-</sup> respectively.

volumes in vehicle-treated WT versus *Cldn16*<sup>-/-</sup> mice (Figure 2A). Furosemide induced significant increases in urine volumes in both genotypes (WT: +0.06 ml/g body weight×24h,  $p < 0.01$ ; *Cldn16*<sup>-/-</sup>: +0.07 ml/g body weight×24h,  $p < 0.01$ ; Figure 2A), which was paralleled by significant decreases of urine osmolalities (WT: from 1655.4 to 823.3 mOsmol,  $p < 0.05$ ; *Cldn16*<sup>-/-</sup>: from 2029.0 to 881.3 mOsmol,  $p < 0.01$ ). Creatinine clearance (CrCl) showed no significant differences between vehicle-treated WT and *Cldn16*<sup>-/-</sup> mice and furosemide produced no significant changes in CrCl as well (Figure 2B). Renal electrolyte handling was assessed by means of mass electrolyte excretion and their fractional excretion rates (FE). Compared to vehicle-treated WT mice, vehicle-treated *Cldn16*<sup>-/-</sup> mice exhibited significantly increased mass excretion of  $\text{Ca}^{2+}$  (+3.5 mg/kg body weight×24h,  $p < 0.0001$ ),  $\text{Mg}^{2+}$  (+3.0 mg/kg body weight×24h,  $p < 0.0001$ ),  $\text{K}^+$  (+8.1 mmol/kg body weight×24h,  $p < 0.001$ ), phosphate (+6.7 mg/kg body

weight×24h,  $p < 0.001$ ), and  $\text{Cl}^-$  (+6.5 mmol/kg body weight×24h,  $p < 0.001$ ), whereas excretion of  $\text{Na}^+$  was not altered (Table 1). Furosemide significantly increased the mass excretion of  $\text{Ca}^{2+}$  (+0.5 mg/kg body weight/24h,  $p < 0.01$ ),  $\text{K}^+$  (+5.9 mmol/kg body weight/24h,  $p < 0.05$ ),  $\text{Na}^+$  (+5.5 mmol/kg body weight/24h,  $p < 0.001$ ), and  $\text{Cl}^-$  (+7.5 mmol/kg body weight/24h,  $p < 0.0001$ ) but did not affect the excretion of  $\text{Mg}^{2+}$  or phosphate in WT (Table 1). In contrast to WT mice, *Cldn16*<sup>-/-</sup> mice responded to furosemide with significantly reduced mass excretion of  $\text{Ca}^{2+}$  (-1.4 mg/kg body weight/24h,  $p < 0.01$ ), whereas excretion of  $\text{Na}^+$  was significantly increased (+2.7 mmol/kg body weight/24h,  $p < 0.01$ ) and other electrolytes were not significantly affected by furosemide (Table 1). Parallel calculation of fractional electrolyte excretion rates for the divalent cations revealed increased  $\text{FE}_{\text{Ca}^{2+}}$  (+9.6%,  $p < 0.001$ ) and  $\text{FE}_{\text{Mg}^{2+}}$  (+21.2%,  $p < 0.01$ ) in vehicle-treated *Cldn16*<sup>-/-</sup> compared to WT controls (Figure 2C,D).  $\text{FE}_{\text{Ca}^{2+}}$  was not significantly changed by furosemide in WT mice,

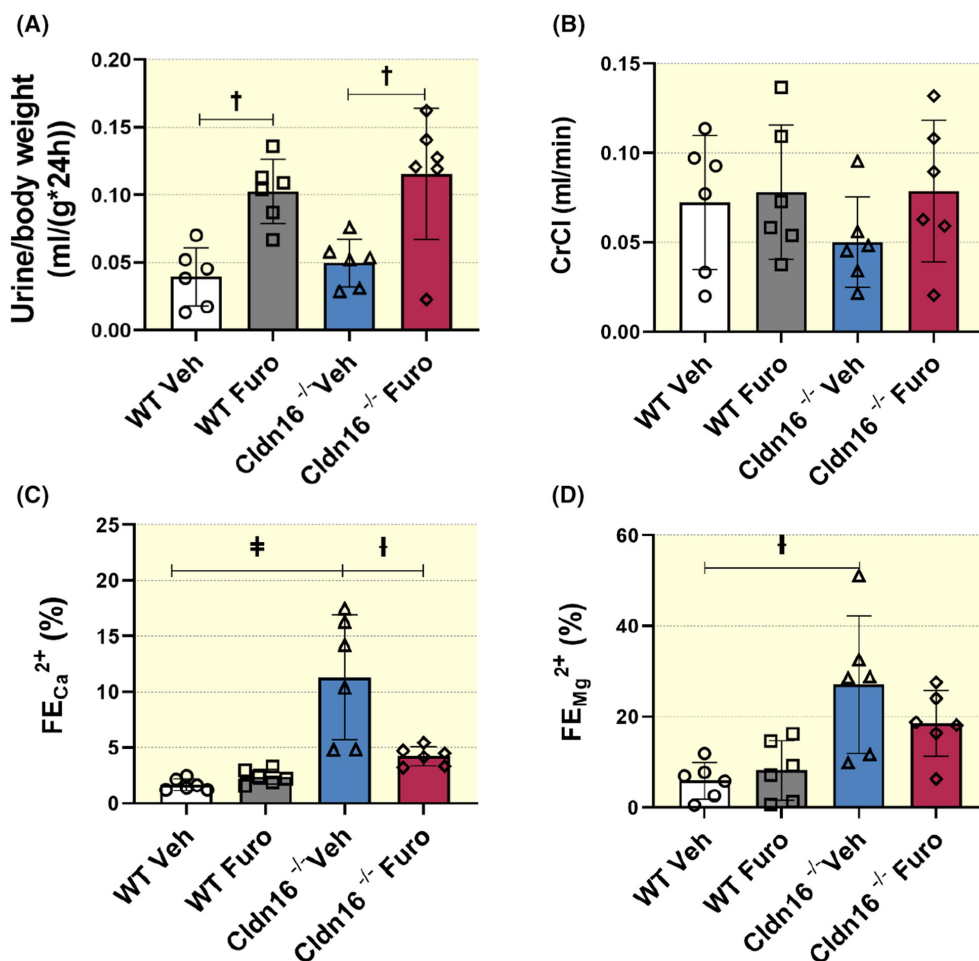


**FIGURE 2** Effects of furosemide (Furo) on renal urinary parameters in wild-type (WT) versus claudin-16 knockout mice (*Cldn16*<sup>-/-</sup>). (A–D) The graphs show comparative analysis of urine volume (A), creatinine clearance (CrCl) (B), and fractional excretion of calcium ( $\text{FE}_{\text{Ca}^{2+}}$ ) (C) and magnesium ( $\text{FE}_{\text{Mg}^{2+}}$ ) (D) obtained from wild-type (WT) and claudin-16 knockout mice (*Cldn16*<sup>-/-</sup>) treated with vehicle (Veh) or Furo;  $N = 6$  in each group. The data are the means ± standard deviations, \* $p < 0.05$ , † $p < 0.01$ , ‡ $p < 0.001$ , ns – not significant, one-way (ANOVA) analysis of variance followed by Tukey's multiple comparisons test.



**TABLE 1** Renal electrolyte handling in wild-type (WT) and Cldn16-knockout mice (KO) treated with vehicle (Veh) or furosemide (Furo)

|                                | WT Veh       | WT Furo        | KO Veh                     | KO Furo                       |
|--------------------------------|--------------|----------------|----------------------------|-------------------------------|
| Body weight (g)                | 32.8 ± 1.3   | 29.3 ± 2.8     | 30.2 ± 1.8                 | 29.5 ± 1.5                    |
| <i>Serum parameters</i>        |              |                |                            |                               |
| Na <sup>+</sup> (mmol/L)       | 153.2 ± 1.7  | 153.3 ± 1.9    | 156.5 ± 1.8 <sup>#</sup>   | 157.2 ± 2.2 <sup>#</sup>      |
| K <sup>+</sup> (mmol/L)        | 5.9 ± 0.6    | 6.8 ± 1.4      | 6.4 ± 0.8                  | 7.2 ± 1.4                     |
| Cl <sup>-</sup> (mmol/L)       | 111.7 ± 11.6 | 115.7 ± 5.4    | 115.5 ± 7.0                | 114.6 ± 7.7                   |
| Ca <sup>2+</sup> (mmol/L)      | 2.3 ± 0.05   | 2.2 ± 0.02     | 2.3 ± 0.1                  | 2.4 ± 0.05 <sup>##</sup>      |
| Mg <sup>2+</sup> (mmol/L)      | 1.4 ± 0.1    | 1.2 ± 0.2      | 1.2 ± 0.1                  | 1.3 ± 0.2                     |
| Phosphate (mg/dl)              | 8.2 ± 1.4    | 8.6 ± 1.0      | 9.9 ± 4.5                  | 8.4 ± 1.0                     |
| Creatinine (mg/dl)             | 0.22 ± 0.02  | 0.20 ± 0.02    | 0.25 ± 0.02 <sup>#</sup>   | 0.22 ± 0.05                   |
| <i>Urine parameters</i>        |              |                |                            |                               |
| <i>1st day</i>                 |              |                |                            |                               |
| Osmolality (mosm/kg)           | 1133.2 ± 396 | 896.3 ± 207    | 1434.2 ± 147               | 1112.2 ± 398                  |
| Ca <sup>2+</sup> (mg/kg/24 h)  | 0.2 ± 0.1    | 0.8 ± 0.4*     | 2.2 ± 0.9 <sup>###</sup>   | 1.4 ± 0.8                     |
| Mg <sup>2+</sup> (mg/kg/24 h)  | 0.6 ± 0.5    | 1.3 ± 1.4      | 2.3 ± 0.8 <sup>###</sup>   | 2.1 ± 0.8                     |
| K <sup>+</sup> (mmol/kg/24 h)  | 6.4 ± 4.0    | 14.2 ± 5.7*    | 11.6 ± 4.1                 | 14.1 ± 2.4**                  |
| Na <sup>+</sup> (mmol/kg/24 h) | 4.1 ± 2.4    | 10.0 ± 2.5**   | 5.6 ± 2.5                  | 7.8 ± 1.2**                   |
| Phosphate (mg/kg/24 h)         | 1.4 ± 1.3    | 3.7 ± 2.7      | 6.1 ± 1.9 <sup>###</sup>   | 6.9 ± 4.5                     |
| Cl <sup>-</sup> (mmol/kg/24 h) | 5.8 ± 3.8    | 13.3 ± 4.2**   | 9.6 ± 3.5                  | 11.1 ± 1.6                    |
| <i>7th day</i>                 |              |                |                            |                               |
| Osmolality (mosm/kg)           | 1655.4 ± 683 | 823.3 ± 279*   | 2029.0 ± 425               | 881.3 ± 125**                 |
| Ca <sup>2+</sup> (mg/kg/24 h)  | 0.2 ± 0.08   | 0.7 ± 0.3**    | 3.7 ± 0.8 <sup>####</sup>  | 2.3 ± 0.6** <sup>###</sup>    |
| Ca <sup>2+</sup> (mg/dl)       | 7.2 ± 3.4    | 7.9 ± 3.6      | 66.0 ± 5.7 <sup>####</sup> | 23.9 ± 4.7*** <sup>####</sup> |
| Mg <sup>2+</sup> (mg/kg/24 h)  | 0.5 ± 0.3    | 1.2 ± 1.2      | 3.5 ± 0.5 <sup>####</sup>  | 2.8 ± 0.9 <sup>#</sup>        |
| K <sup>+</sup> (mmol/kg/24 h)  | 6.2 ± 1.8    | 12.1 ± 3.9*    | 14.3 ± 2.6 <sup>###</sup>  | 16.2 ± 1.9                    |
| Na <sup>+</sup> (mmol/kg/24 h) | 4.0 ± 2.3    | 9.5 ± 1.4***   | 5.2 ± 1.3                  | 7.9 ± 1.1**                   |
| Phosphate (mg/kg/24 h)         | 1.6 ± 0.7    | 2.8 ± 3.9      | 8.3 ± 1.6 <sup>###</sup>   | 6.6 ± 1.6                     |
| Cl <sup>-</sup> (mmol/kg/24 h) | 5.6 ± 1.8    | 13.1 ± 2.9**** | 12.1 ± 2.1 <sup>###</sup>  | 13.2 ± 1.4                    |

Note: Analysis of body weight, serum electrolytes, serum creatinine, urinary excretion of electrolytes, and urinary Ca<sup>2+</sup> concentrations in wild-type (WT) and Claudin 16-deficient mice (KO) treated with vehicle (Veh) or furosemide (Furo) for 1 or 7 days. \* $p < 0.05$ , \*\* $p < 0.01$ , \*\*\* $p < 0.001$ , \*\*\*\* $p < 0.0001$  for differences between the treatment groups of the same genotype (vehicle and furosemide-treated KO mice). <sup>#</sup> $p < 0.05$ , <sup>##</sup> $p < 0.01$ , <sup>###</sup> $p < 0.001$ , <sup>####</sup> $p < 0.0001$  for differences between the two genotypes receiving the same treatment (vehicle-treated WT and KO animals, or furosemide-treated WT and KO animals).

whereas Cldn16<sup>-/-</sup> demonstrated a marked FE<sub>Ca</sub><sup>2+</sup> reduction upon furosemide application (-7.1%,  $p < 0.01$ ; Figure 2C). In line with this, the urinary Ca<sup>2+</sup> concentration was substantially higher in vehicle-treated Cldn16<sup>-/-</sup> compared to the WT controls (+58.8 mg/dl,  $p < 0.0001$ ; Table 1). Furosemide did not alter the urinary Ca<sup>2+</sup> concentration in WT but significantly reduced this value in Cldn16<sup>-/-</sup> (-42.1 mg/dl,  $p < 0.001$ ; Table 1). FE<sub>Mg</sub><sup>2+</sup> was not significantly changed by furosemide either in WT or Cldn16<sup>-/-</sup> (Figure 2D). Analysis of serum electrolyte concentrations revealed mild hypernatremia in vehicle- and furosemide-treated Cldn16<sup>-/-</sup> mice compared to the respective WT groups (Table 1). Serum K<sup>+</sup>, Cl<sup>-</sup>, Mg<sup>2+</sup>, and phosphate levels were similar across the genotypes and

treatment groups, except of slightly increased Ca<sup>2+</sup> level in furosemide-treated Cldn16<sup>-/-</sup> compared to furosemide-treated WT mice (Table 1).

In addition to the chronic effects of furosemide, we have measured urinary electrolyte excretion on the first day of treatment to assess the acute effects of the diuretic. The results were largely similar to the data obtained after 7 days of furosemide application, although the furosemide-induced reduction of urinary Ca<sup>2+</sup> excretion in Cldn16<sup>-/-</sup> did not reach the statistical significance (Table 1).

Based on these results we concluded that Cldn16<sup>-/-</sup> exhibit an FHHNC-like phenotype and chronic furosemide treatment alleviates the urinary Ca<sup>2+</sup> loss in Cldn16-deficiency.

## 2.2 | Effects of furosemide on distal $\text{Ca}^{2+}$ and $\text{Mg}^{2+}$ transport systems in WT versus *Cldn16*-deficient mice

Next, we evaluated the potential mechanisms underlying the furosemide-induced improvement of renal  $\text{Ca}^{2+}$  handling in *Cldn16*<sup>-/-</sup>. Analysis of distal  $\text{Ca}^{2+}$  and  $\text{Mg}^{2+}$  transport systems using quantitative PCR (qPCR) showed enhanced expression of TRPM6 (+97%,  $p < 0.05$ ), TRPV5 (+236,  $p < 0.05$ ), parvalbumin (Pva) (+91,  $p < 0.05$ ), and Calb (+324%,  $p < 0.001$ ) in kidney lysates from vehicle-treated *Cldn16*<sup>-/-</sup> compared to WT mice (Figure 3A–D). Furosemide did not significantly alter the expression of either product in WT mice. *Cldn16*<sup>-/-</sup> responded to furosemide with a further increase of TRPV5 expression (+257%,  $p < 0.05$ ), whereas the mRNA levels of TRPM6, Pva, and Calb were not significantly altered (Figure 3A–D).

Next, we evaluated luminal and basolateral  $\text{Ca}^{2+}$  or  $\text{Mg}^{2+}$  transport proteins by immunoblotting. In line with

the results of qPCR, immunoblotting analysis showed increased TRPM6 abundance in kidneys from *Cldn16*<sup>-/-</sup> compared to WT controls and no significant effects of furosemide in either genotype (Figure 4A–E). Since NCC may indirectly affect luminal entry of divalent cations, we have compared its levels between the genotypes and treatment groups as well. No significant differences in NCC levels were detected between vehicle-treated WT and *Cldn16*<sup>-/-</sup> mice, whereas furosemide induced compensatory increases of its abundance in both genotypes (WT: +65%,  $p < 0.001$ ; *Cldn16*<sup>-/-</sup>: +46%,  $p < 0.01$ ; Figure 4A–D,F). PMCA protein levels were not different in WT and *Cldn16*<sup>-/-</sup> mice. Furosemide induced a significant increase of PMCA abundance in *Cldn16*<sup>-/-</sup> (+296%,  $p < 0.01$ ) but not in WT mice, which resulted in higher PMCA levels in furosemide-treated *Cldn16*<sup>-/-</sup> mice compared to the furosemide-treated WT controls (+189%,  $p < 0.01$ ; Figure 5A–E). In contrast, NCX1 protein levels were moderately increased in *Cldn16*<sup>-/-</sup> mice at baseline

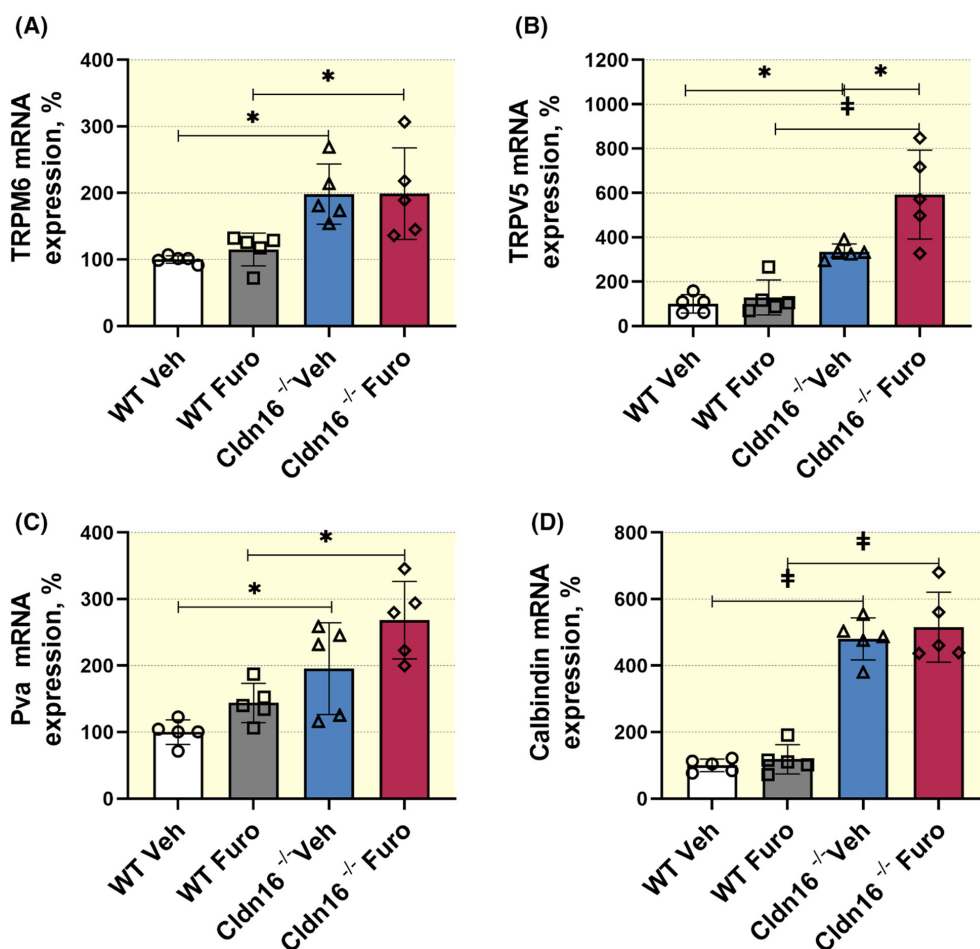


**FIGURE 3** Effects of furosemide (Furo) on expression of distal divalent cation transport proteins. (A–D) Graphs show results of quantitative PCR analysis of mRNA levels of the transient receptor potential (TRP) channels, TRPV5 and TRPM6, parvalbumin (Pva), and calbindin in kidney lysates from wild-type (WT) and claudin-16 knockout (*Cldn16*<sup>-/-</sup>) mice treated with vehicle (Veh) or furosemide (Furo).  $N = 5$  in each group. The data are the means  $\pm$  standard deviations, \* $p < 0.05$ , † $p < 0.001$ , ns – not significant, one-way (ANOVA) analysis of variance followed by Tukey's multiple comparisons test.

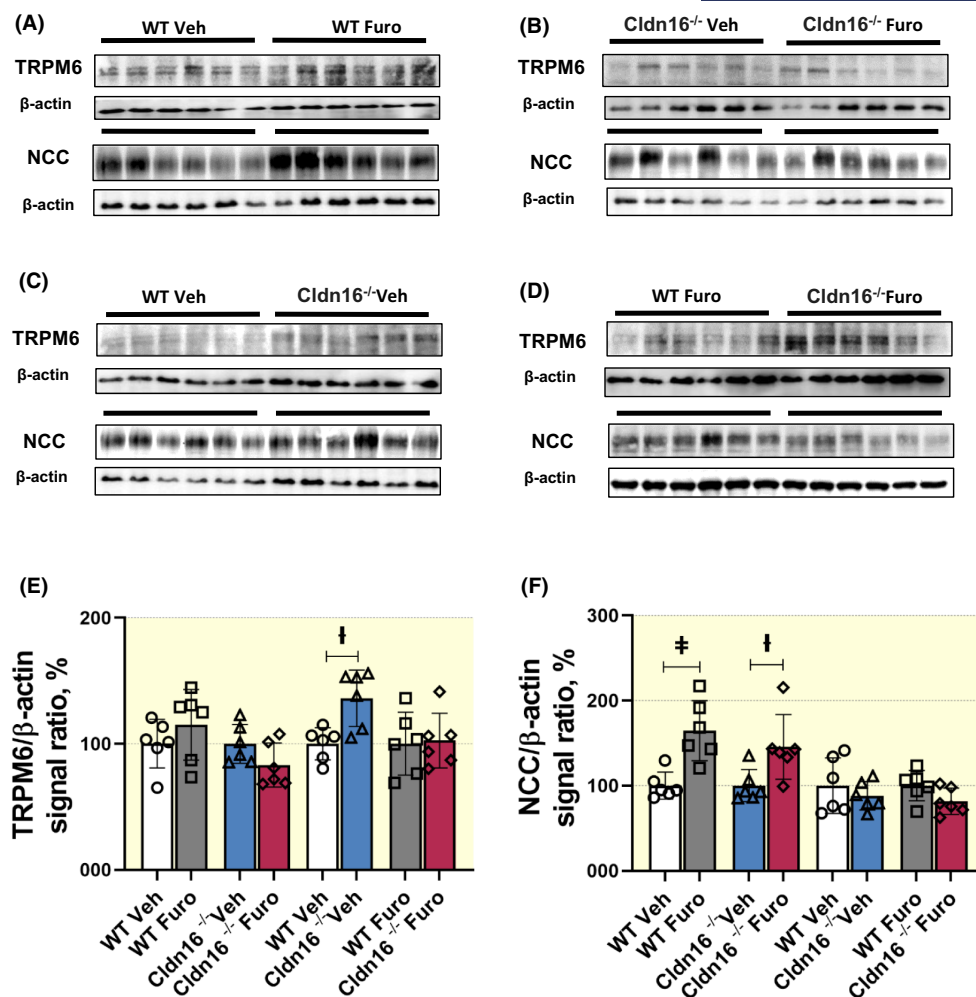


**FIGURE 4** Effects of furosemide (Furo) on the protein abundance of the transient receptor potential melastatin 6 (TRPM6) and Na<sup>+</sup>, Cl<sup>-</sup> cotransporter (NCC) as detected by immunoblotting. (A–D) Representative immunoblots for TRPM6 (approximately 234 kDa) and NCC (approximately 160 kDa) obtained with kidney lysates from wild-type (WT) and claudin-16 knockout (Cldn16<sup>-/-</sup>) mice treated with vehicle (Veh) or furosemide (Furo); β-Actin detection served for the loading control,  $N = 6$  in each group. (E,F) Graphs show densitometric evaluation of TRPM6 (E) or NCC (F) signals after normalization for β-Actin. The data are the means  $\pm$  standard deviations,  $^{\dagger}p < 0.01$ ,  $^{\ddagger}p < 0.001$ , ns – not significant,  $t$  test.

(+25%,  $p < 0.05$ ) but furosemide did not augmented its abundance in WT or Cldn16<sup>-/-</sup> mice (Figure 5A–D,F). Accordingly, a moderately higher NCX1 abundance was also observed in Cldn16<sup>-/-</sup> after the furosemide treatment reflecting the increase obtained at baseline (+53%,  $p < 0.01$ ; Figure 5A–D,F).

Protein evaluation for TRPV5 and Calb was performed using immunofluorescence rather than by immunoblotting due to poor signal/background ratios obtained with the latter method. At the qualitative level, whole kidney imaging demonstrated higher fractional volumes of TRPV5-positive and Calb-positive tubules in the renal cortex of vehicle-treated Cldn16<sup>-/-</sup> kidneys compared to the WT controls (Figure 6A,C, Figure S1A,C). Furosemide induced no obvious changes in TRPV5 signal abundance in WT kidneys but visibly enhanced the fraction of TRPV5-positive renal tubules in Cldn16<sup>-/-</sup> kidneys

(Figure 6A–D). In contrast, the Calb signal was not affected by furosemide in either WT or Cldn16<sup>-/-</sup> mice (Figure S1A–D). Detailed analysis of TRPV5 distribution using immunofluorescence and confocal microscopy showed a moderate TRPV5 signal predominantly in the late DCT (DCT2) and to a lesser extent in CNT/cortical CD (cCD) of vehicle-treated WT mice, as identified by double-labeling of CNT/cCD using an antibody to aquaporin 2 (AQP2) (Figure 7A). Furosemide did not significantly change this distribution pattern in WT kidneys (Figure 7B). In contrast to WT, vehicle-treated Cldn16<sup>-/-</sup> exhibited an intensive TRPV5 signal throughout the DCT2, CNT, and cCD, as identified by double-labeling for AQP2 (Figure 7C). Furosemide further enhanced the TRPV5 signal (Figure 7D). Moreover, a moderate TRPV5 signal was also detected in principal cells (PCs) of the outer medullary CD (omCD) in furosemide-treated Cldn16<sup>-/-</sup> only

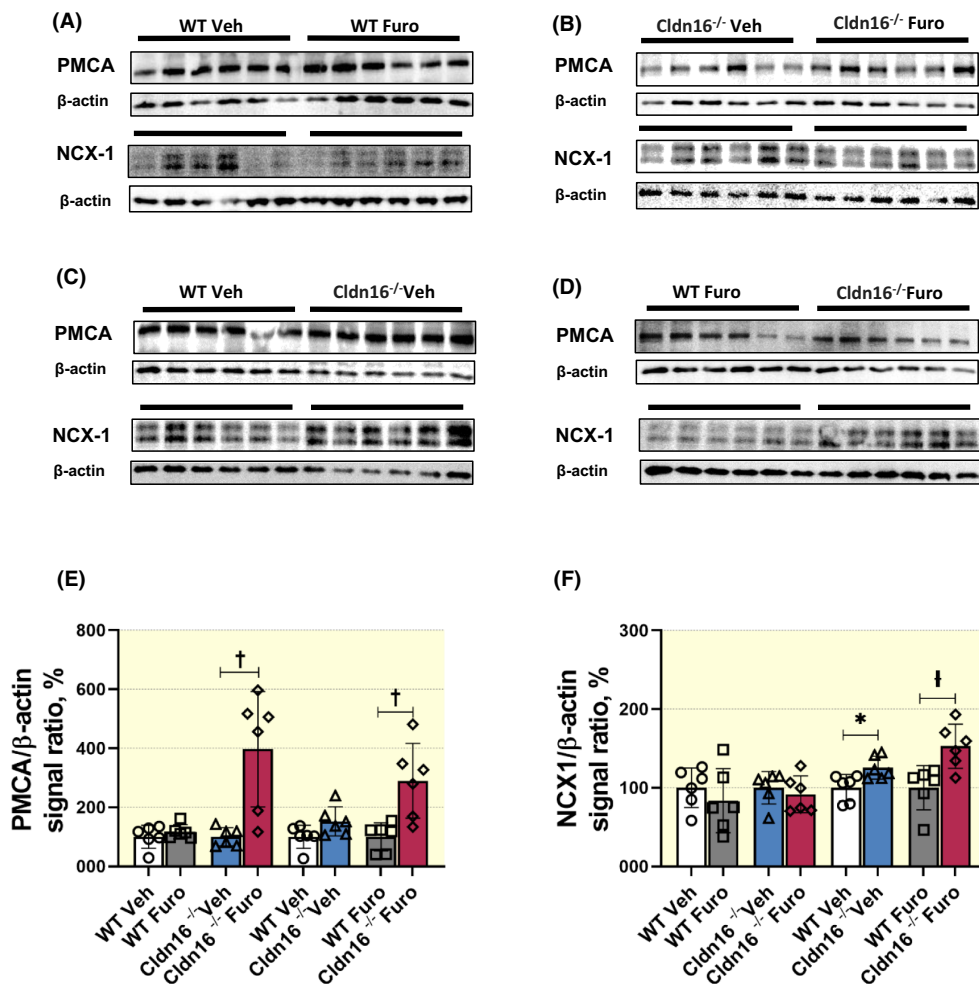


**FIGURE 5** Effects of furosemide (Furo) on protein abundance of the plasma membrane calcium ATPase (PMCA) and sodium-calcium exchanger (NCX1) as detected by immunoblotting. (A–D) Representative immunoblots for PMCA (approximately 150 kDa) and NCX1 (approximately 120 kDa) obtained with kidney lysates from wild-type (WT) and claudin-16 knockout (Cldn16<sup>-/-</sup>) mice treated with vehicle (Veh) or furosemide (Furo); β-actin detection served for the loading control,  $N = 6$  in each group. (E,F) Graphs show densitometric evaluation of PMCA (E) or NCX1 (F) signals after normalization for β-actin. The data are the means ± standard deviations, † $p < 0.01$ , ‡ $p < 0.001$ , ns – not significant,  $t$  test.

(Figure S2A–D). Therefore, furosemide treatment stimulated TRPV5 and PMCA in Cldn16<sup>-/-</sup> mice, which may underlie the furosemide-induced reduction of  $\text{FE}_{\text{Ca}}^{2+}$  in this FHHNC model.

### 2.3 | Effects of furosemide on proximal $\text{Ca}^{2+}$ and $\text{Mg}^{2+}$ transport systems in WT versus Cldn16-deficient mice

Since the major part of filtered  $\text{Ca}^{2+}$  is reabsorbed in PT via the paracellular route, we have next evaluated the claudin 2 (Cldn2) mediating the proximal reabsorption of divalent cations.<sup>8,21</sup> Immunoblotting revealed increased Cldn2 abundance in kidney lysates from vehicle-treated Cldn16<sup>-/-</sup> compared to vehicle-treated WT mice (+49%,  $p < 0.01$ ; Figure 8A,B). Furosemide increased the Cldn2

abundance in WT (+17%,  $p < 0.05$ ) but did not change the Cldn2 protein level in Cldn16<sup>-/-</sup>. As a result, furosemide-treated WT and Cldn16<sup>-/-</sup> exhibited similar Cldn2 protein levels (Figure 8A,B). Since NHE3 may modulate the calcium reabsorption along the proximal tubule,<sup>22</sup> we have evaluated its abundance as well. Baseline NHE3 levels were not different between vehicle/treated WT and Cldn16<sup>-/-</sup> mice. Upon furosemide, Cldn16<sup>-/-</sup> mice exhibited a trend for decreased NHE3 levels, which was reflected by decreased NHE3 abundance upon furosemide (Figure 8A–D,F).

## 3 | DISCUSSION

FHHNC patients suffer from polyuria, polydipsia, enuresis, as well as recurrent urinary tract infections.<sup>7</sup> The



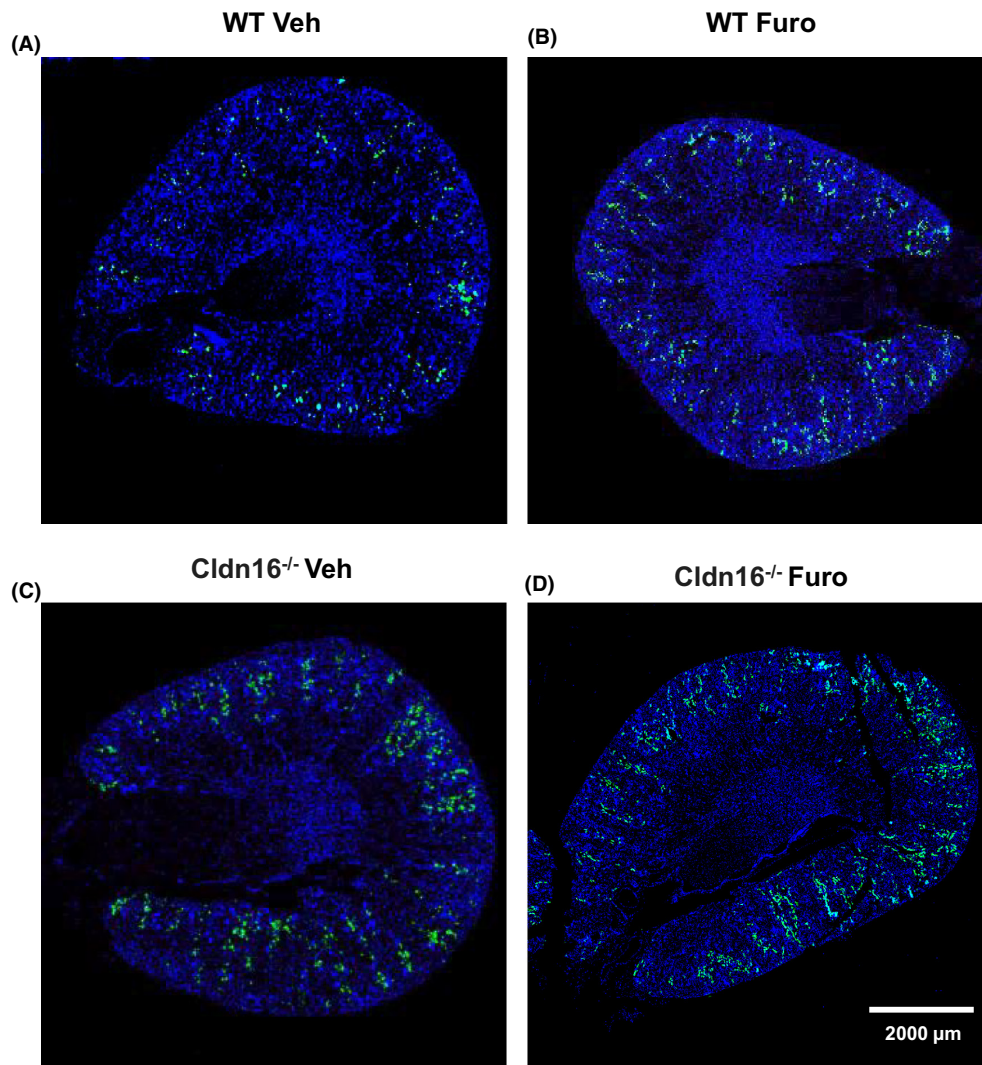


**FIGURE 6** Effects of furosemide (Furo) on the protein abundance of transient receptor potential vanilloid 5 (TRPV5) as detected by immunofluorescence. (A–D) Representative whole kidney images showing the abundance of TRPV5-positive renal tubules (green signal) in kidneys of wild-type (WT) or claudin-16 knockout mice (Cldn16<sup>-/-</sup>) treated with vehicle (Veh) or furosemide (Furo); nuclei are counterstained with DAPI (blue signal);  $N = 4$  in each group. Note increased TRPV5 signal abundance in vehicle-treated Cldn16<sup>-/-</sup> mice compared to vehicle-treated WT mice (A,C) and a further stimulation of TRPV5 by furosemide (B,D).

foremost factor limiting their life expectancy is calcium dysregulation causing nephrocalcinosis, nephrolithiasis, and CKD. Serum  $Mg^{2+}$  levels can be unaffected.<sup>6</sup> The present results put forward furosemide treatment as an effective measure to restore the calcium homeostasis. Current therapeutic strategies based on thiazide diuretics or indomethacin fail to normalize urinary  $Ca^{2+}$  excretion, thus, nephrocalcinosis still occurs.<sup>6,7</sup>

Although thiazides are traditionally used for treatment of hypercalciuria and prevention of nephrolithiasis,<sup>23</sup> the mechanisms underlying their effects on renal  $Ca^{2+}$  handling remain unclear. Thiazide diuretics may cause volume contraction with a modest decrease in GFR. The latter enhances NaCl reabsorption in the proximal nephron and augments the impact of the proximal tubule on  $Ca^{2+}$  reabsorption.<sup>24,25</sup> Alternatively, thiazides

may directly enhance  $Ca^{2+}$  reabsorption in DCT cells via hyperpolarization of the plasma membrane and increased drive for cation influx.<sup>26,27</sup> However, chronic NCC inhibition may cause apoptosis in DCT cells thereby reducing the DCT mass and decreasing its impact on the reabsorption of divalent cations.<sup>28,29</sup> Thus, hypocalciuric effects of thiazide diuretics in patients are likely related to volume contraction, compensatory changes in GFR and increase of  $Ca^{2+}$  reabsorption along the PT, whereas the distal  $Ca^{2+}$  reabsorption may be unaffected or even decreased due to reduction of DCT mass.<sup>24,28–30</sup> Moreover, chronic pharmacological suppression or deletion of NCC in mice is associated with reduced TRPM6 expression and hypomagnesemia, which may result from destructive morphological changes in DCT1.<sup>24,28,31</sup> Taken together, the therapeutic

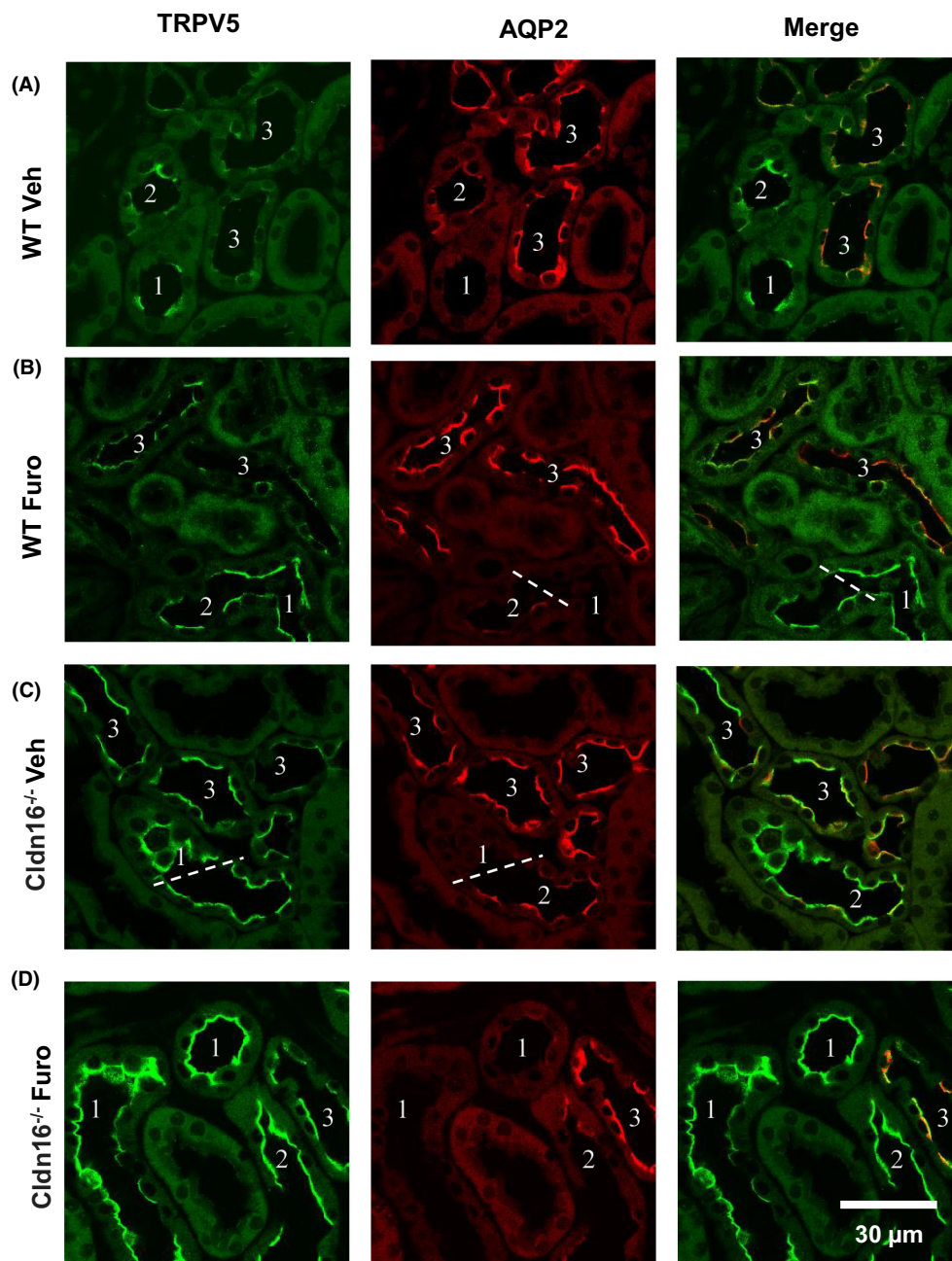


**FIGURE 7** Effects of furosemide (Furo) on the distribution of the transient receptor potential vanilloid 5 (TRPV5) in kidney cortex as detected by confocal microscopy. (A–D) Representative confocal microscopic images of renal cortical regions showing double-labeling of transient receptor potential vanilloid 5 (TRPV5, green signal) and aquaporin 2 (AQP2, red signal) in kidney sections from wild-type (WT) and claudin-16 knockout mice (Cldn16 KO) treated with vehicle (Veh) or furosemide (Furo). Both Veh- (A) or furosemide-treated WT kidneys (B) show TRPV5 signal predominantly in AQP2-negative late distal convoluted tubules (DCT2, 1) and to a lesser extent in AQP2-positive connecting tubules (CNT, 2) or cortical collecting ducts (cCD, 3). Compared to WT, Veh-treated Cldn16 KO mice show a stronger TRPV5 signal in both DCT2 and CNT/cCD (C). Furosemide led to a further increase of the TRPV5 signal intensity in Cldn16 KO kidneys (D).  $N = 4$  per treatment group, scale bar: 30  $\mu\text{m}$ .

action of thiazide diuretics in FHHNC patients may be limited by their side effects including chronic reduction of GFR, hypomagnesemia, and apoptosis of DCT1 with sterile interstitial inflammation.

Cldn10 deletion corrects the FHHNC-like phenotype of Cldn16<sup>-/-</sup>.<sup>20</sup> These double-knockout mice exhibit

polyuria due to impaired transport function of TAL. Moreover, signs of compensatory hypertrophy are evident in the ensuing distal nephron segments.<sup>20</sup> This phenotype led us to assume that pharmacological inhibition of NaCl reabsorption in TAL by furosemide can rescue hypercalciuria in FHHNC patients. Furosemide

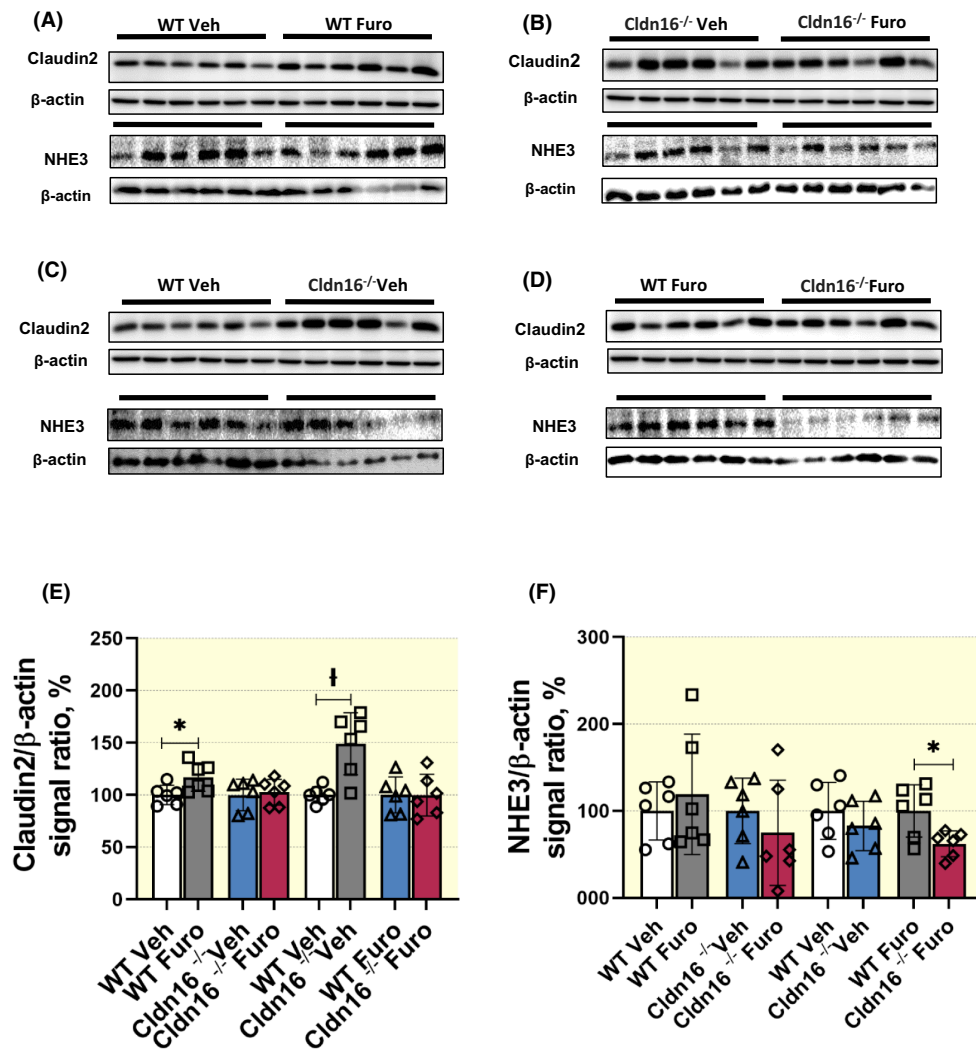


**FIGURE 8** Effects of furosemide (Furo) on the claudin-2 and NHE3 as detected by immunoblotting. (A–D) Representative immunoblots for claudin-2 (approximately 25 kDa) and NHE3 (approximately 85 kDa) obtained from kidney lysates of wild-type (WT) and claudin-16 knockout (Cldn16<sup>-/-</sup>) mice treated with vehicle (Veh) or furosemide (Furo);  $\beta$ -Actin detection served for the loading control,  $N = 6$  in each group. (E,F) Graphs show densitometric evaluation of respective immunoreactive signals after normalization to  $\beta$ -Actin. The data are the means  $\pm$  standard deviations, \* $p$  < 0.05,  $^{\dagger}$  $p$  < 0.01, ns – not significant,  $t$  test.

causes the opposite effect, that is, hypercalciuria, in patients and animal models by decreasing paracellular reabsorption of divalent cations along the TAL.<sup>3,4,18,32</sup> In FHHNC patients, however, this undesired effect may not take place due to the severely reduced paracellular permeability in TAL caused by inactivating mutations in CLDN16 or CLDN19 genes.<sup>6,7</sup> Quite the contrary, in this disease state, furosemide-induced increase of NaCl load in the ensuing nephron segments may stimulate their compensatory activation including the transcellular  $\text{Ca}^{2+}$  reabsorption.<sup>20</sup> To test our hypothesis we have used Cldn16<sup>-/-</sup> as an FHHNC model.

Cldn16<sup>-/-</sup> mice mimic FHHNC by urinary  $\text{Ca}^{2+}$  and  $\text{Mg}^{2+}$  wasting. Stimulated distal divalent cation transport partially compensates the losses.<sup>4,20</sup> We detected a proximal compensatory mechanism, enhanced Cldn2

abundance, suggesting increased paracellular permeability for  $\text{Ca}^{2+}$  along the PT.<sup>8,33</sup> Apart from Cldn2, Cldn12 has also been implicated in reabsorption of divalent cations in the proximal tubule.<sup>33</sup> Although the impact of Cldn12 on the calcium reabsorption appears to be lower compared to Cldn2,<sup>8,34,35</sup> the contribution of Cldn12 may be compensatory increased in Cldn16-deficiency. This potential mechanism should be addressed in future studies.

Increased  $\text{K}^{+}$  excretion observed in Cldn16<sup>-/-</sup> in the present study points to a compensatory reaction in CNT/CD. This result is in line with the previously published renal phenotype of Cldn16-knockdown mice. These have impaired paracellular cation reabsorption in TAL, increased  $\text{FE}_{\text{Na}}^{+}$  and  $\text{FE}_{\text{Cl}}^{-}$ , lower blood pressure, enhanced epithelial sodium channel (EnaC) activity, and stronger response to amiloride compared to WT.<sup>36</sup> Interestingly,



the present and previous studies provide no indications for compensatory upregulation of NaCl reabsorption in DCT of *Cldn16*<sup>-/-</sup> mice, as evident from the analysis of total and phosphorylated NCC.<sup>20</sup> Instead, enhanced *Cldn2* abundance may compensate for distal sodium loss, since *Cldn2* is permeable both for mono- and divalent cations.<sup>21</sup> Finally, NHE3 mediates proximal Na<sup>+</sup> reabsorption and indirectly promotes the Ca<sup>2+</sup> reabsorption as well.<sup>37</sup> However, its abundance was decreased rather than increased in *Cldn16*<sup>-/-</sup> mice receiving furosemide, thus excluding its role in compensation of the urinary Ca<sup>2+</sup> loss in our model.

The most pronounced effect of furosemide in *Cldn16*<sup>-/-</sup> is the reduction of urinary calcium excretion, both mass excretion and  $\text{FE}_{\text{Ca}}^{2+}$ . To test the role of proximal tubule herein, we measured CrCl and *Cldn2* abundance. CrCl, as an approximate to GFR, was unaffected by furosemide in both genotypes and *Cldn2* abundance increased in WT only. Since the CrCl is an unreliable parameter to estimate GFR in mice,<sup>38</sup> compensatory changes in GFR cannot be ruled out. However, furosemide has been shown to suppress the tubuloglomerular feedback without concomitant changes in GFR or proximal reabsorption.<sup>39</sup> It is tempting to speculate that furosemide does not increase the proximal Ca<sup>2+</sup> reabsorption in *Cldn16*<sup>-/-</sup> mice either via decrease of GFR or stimulation of paracellular Ca<sup>2+</sup> transport via *Cldn2*. Nonetheless, the effect of furosemide on *Cldn12* still needs to be studied.

In contrast to the proximal mechanisms, treatment of *Cldn16*<sup>-/-</sup> mice with furosemide stimulated the distal Ca<sup>2+</sup> transport pathways, PMCA (likely PMCA4)<sup>15</sup> and TRPV5, which may limit the calcium wasting in this FHHNC model. Notably, furosemide did not affect these proteins in WT mice, which may be related to recruitment of the proximal tubular compensatory mechanisms, as reflected by increased *Cldn2* abundance. Although the role of PMCA in urinary calcium excretion remains debatable,<sup>15,40</sup> our data suggest that stimulation of this basolateral calcium transport pathway by furosemide may contribute to compensation of the hypercalciuria in FHHNC. TRPV5 is critical to the renal Ca<sup>2+</sup> reabsorption.<sup>13,41</sup> Apart from enhanced TRPV5 mRNA expression, furosemide increased the fractional volume of TRPV5-expressing renal tubules in *Cldn16*-deficient kidneys, indicating compensatory nephron remodeling, as shown for other models.<sup>42–44</sup> Nephron remodeling may include hypertrophy or hyperplasia of certain distal nephron segments. However, analysis of calbindin revealed no expansion of calbindin-expressing DCT2 or CNT/cCD in response to furosemide.<sup>45</sup> Phenotyping of the TRPV5-expressing cells using double-labeling for AQP2 demonstrated a higher proportion of TRPV5-expressing principal cells (PCs) in CNT/cCD, which was further increased after

furosemide treatment reaching the PCs of omCD. Prior work suggested that the activity of TRPV5 promoter is limited to DCT2, CNT and initial cCD,<sup>46</sup> whereas the present results clearly demonstrate recruitment of PCs along the entire cCD and initial omCD. To our knowledge, the present study provides new evidence for the functional plasticity of CD with respect to the Ca<sup>2+</sup> reabsorption. The present results suggest that furosemide-induced stimulation of the TRPV5-mediated distal Ca<sup>2+</sup> reabsorption reflects functional remodeling along the distal nephron and CD contributing to alleviation of the urinary Ca<sup>2+</sup> wasting in *Cldn16*<sup>-/-</sup> mice. Furosemide prevents entry of Na<sup>+</sup>, K<sup>+</sup>, and Cl<sup>-</sup> into TAL cells, thereby increasing their luminal concentrations downstream. Compensatory activation of the later nephron portions involves Ca<sup>2+</sup> reabsorption parallel to the NaCl transport. The underlying mechanisms may combine endocrine, paracrine, and cell autonomous signaling pathways. Furosemide-induced diuresis and volume contraction may trigger the release of cAMP-generating hormones such as vasopressin or parathyroid hormone (PTH) followed by increase in intracellular cAMP levels and stimulation of protein kinase A-dependent pathways.<sup>47</sup> Since PTH may act via both, intracellular cAMP or Ca<sup>2+</sup> release,<sup>34,47,48</sup> exact mechanisms that trigger PMCA and TRPV5 stimulation in response to furosemide remain to be clarified. In addition, chronic furosemide administration may further affect TRPV5 activity by modulation of the urinary pH.<sup>49,50</sup>

In conclusion, furosemide alleviates calcium wasting in our causal mouse model for FHHNC. Stimulation of distal Ca<sup>2+</sup> transport pathways such as TRPV5 and PMCA may mediate this effect. The present results may have clinical relevance for FHHNC patients.

## 4 | MATERIALS AND METHODS

### 4.1 | Animals

All animal experiments were approved by the German Animal Welfare Regulation Authorities on the protection of animals used for scientific purpose (G0148/18). Generation of claudin-16-deficient mice was described previously.<sup>4</sup> Adult (8 to 10 week-old males) *Cldn16*<sup>-/-</sup> mice and WT littermates were housed under standardized conditions (12 h light/dark cycle, 22–24°C temperature; 55% ± 15% humidity and access to standard diet and water ad libitum). WT (*N* = 24) and *Cldn16*<sup>-/-</sup> mice (*N* = 24) were divided in groups receiving daily intraperitoneal injections of furosemide (40 mg/kg body weight in approximately 0.1 ml 0.9% NaCl) or vehicle for 7 days (*N* = 12 in each group). On the first and last days of the experiment, mice were placed in metabolic cages for 24 h with water



and food ad libitum to collect urine. On the following day, mice were anesthetized (ketamine [100 mg/kg] and xylazine [10 mg/kg], CP-Pharma) to obtain blood sample from the vena cava, followed by in vivo perfusion of the kidneys via the abdominal aorta for morphological studies (6 WT and 6 *Cldn16*<sup>-/-</sup> mice)<sup>51</sup> or kidney removal for biochemical evaluation (6 WT and 6 *Cldn16*<sup>-/-</sup> mice). Blood and urine samples were analyzed in a commercial laboratory (IMD Labor Berlin, Germany). Creatinine clearance (CrCl) was calculated with the standard formula:  $\text{CrCl (ml/min)} = [\text{CU (mg/dl)} \times \text{urine flow (ml/min)}] / \text{CS (mg/dl)}$ , where CU is the concentration of creatinine in the urine and CS is the creatinine concentration in the serum. Fractional excretion rates for electrolytes were calculated using the following formula:  $\text{FE}_{\text{Na}^+} (\%) = 100 \times [\text{NaU (mmol/L)} \times \text{urine flow (ml/min)}] / [\text{CrCl (ml/min)} \times \text{NaS (mmol/L)}]$ , where NaU is the sodium concentration in the urine and NaS is the sodium concentration in the serum.

## 4.2 | Quantitative real-time PCR

Total RNA was extracted from kidney tissue using PeqGOLD TriFast (VWR Life SCIENCE) according to the manufacturer's protocol. Reverse transcription was performed using a Reverse Transcriptase kit (Bioline GmbH) with 1 µg total RNA. Specific forward and reverse primers used for evaluation of the expression of related genes were designed (Table 2). Quantitative real-time PCR (qPCR) was performed using the 7500 Fast Real-Time PCR system (Applied Biosystems) and the HOT FIREPol EvaGreen qPCR Mix (Solis BioDyne). Relative quantity (RQ) of mRNA levels was normalized to endogenous GAPDH. Results were analyzed using the  $\Delta\Delta C_T$  method, and mean values of  $\log_2^{\text{(relative quantification)}}$  from each group were compared.

## 4.3 | Immunofluorescence

Immunofluorescence was performed as described previously.<sup>51</sup> Briefly, paraffin-embedded mouse kidney

sections (4 µm) were dewaxed in xylene followed by rehydration in a graded ethanol series (100%, 96%, 80%, 70%) and boiled in citrate buffer (pH 6) for 6 min for antigen retrieval. Unspecific protein binding was blocked with 5% skim milk or 5% bovine serum albumin in PBS or TBS buffer for 30 min at room temperature. Primary antibodies (Table 3) dissolved in the blocking buffer were applied on the sections for 1 h at room temperature, followed by overnight incubation at +4°C. Signals were visualized using fluorescence-coupled secondary antibodies (1:250; Dianova) and nuclei were counterstained with DAPI (4',6-diamidino-2-phenylindole, Sigma-Aldrich). Evaluation and documentation of immunofluorescence signals were performed by epifluorescence microscopy (Zeiss Axio Imager 2) and confocal microscopy (LSM 5 Exciter, Carl Zeiss Microscopy GmbH).

## 4.4 | Immunoblotting

Whole kidney tissue was homogenized in buffer (250 mM sucrose, 10 mM triethanolamine [AppliChem, PanReac, ITW Reagents]) containing a protease inhibitor cocktail (cOmplete™, Roche). After sonication for 10 s, the samples were centrifuged at 14000×g for 15 min at 4°C to remove cell debris and the supernatant was harvested. Protein concentration of the supernatant was measured by Micro BCA™ protein assay kit (Thermo Scientific). Samples (15 µg per lane) were electrophoretically separated by polyacrylamide gels (10% or 14%), and then transferred to a nitrocellulose membrane (Macherey-Nagel). After blocking with 5% bovine serum albumin in TBST (RT, 30 min), the membranes were incubated with primary antibodies for 1 h at room temperature followed by overnight incubation at +4°C, washing in TBST and subsequent incubation with horseradish peroxidase-(HRP)-conjugated secondary antibodies (Dako; 1:2000) for 1 h at room temperature. Signal was generated by chemiluminescence using Amersham ECL and ChemoCam Imager ECL (Intas Science Imaging). Densitometric evaluation was performed using ImageJ software (National Institutes of Health).

TABLE 2 List of primers used for qPCR analysis

| Gene  | Sequence (forward; reverse)  |
|-------|--|
| GAPDH | 5'-AAC TTT GGC ATT GTG GAA GG-3'; 5'-ACA CAT TGG GGG TAG GAA CA-3' |
| TRPM6 | 5'-CAA CAT TGG AAG CCT GGT GC-3'; 5'-GCT CCG ATA TGC TCC ACC AA-3' |
| TRPV5 | 5'-TGG AGG AGA CCA CCT GAA GT-3'; 5'-GAA CTT GAG GGG GCG GTA AA-3' |
| Pva   | 5'-GCA GAC TCC TTC GAC CAC AA-3'; 5'-TCA GCG CCA CTT AGC TTT CA-3' |
| Calb  | 5'-CAG AAT CCC ACC TGC AGT CA-3'; 5'-GGG TAA GAC GTG AGC CAA CT-3' |

Abbreviations: Calb, calbindin D-28K; GAPDH, glyceraldehyde 3-phosphate dehydrogenase; Pva, parvalbumin; TRPM6, transient receptor potential melastatin 6; TRPV5, luminal transient receptor potential cation channel subfamily V members 5.

TABLE 3 List of the primary antibodies

| Antibody    | Provider   | Host and clonality     | Dilution                   | Catalog number |
|-------------|--|------------------------|----------------------------|----------------|
| NCC         | Sigma-Aldrich  | Rabbit, monoclonal     | 1:1000, 5% BSA/TBST, WB    | AB3553         |
| Occludin    | ThermoFisher Scientific                              | Mouse, monoclonal      | 1:500 IF                   | 33-1500        |
| TRPV5       | Alomone labs   | Rabbit, polyclonal     | 1:1000 IF                  | ACC-035        |
| Calbindin   | Abcam  | Rabbit, monoclonal     | 1:5000 IF                  | Ab108404       |
| TRPM6       | Santa Cruz Biotechnology                             | Mouse, monoclonal      | 1:300, 5% BSA in TBST, WB  | Sc-365536      |
| Claudin 16  | Provided by J Hou                                    | Rabbit, polyclonal     | 1:500 IF                   | –              |
| Parvalbumin | Abcam  | Rabbit, monoclonal     | 1:500, 5% BSA in TBST, WB  | Ab181086       |
| AQP2        | Santa Cruz Biotechnology                             | Goat, polyclonal       | 1:2000 IF                  | C2316          |
| NCX1        | Abcam  | Rabbit, monoclonal     | 1:500, 5% BSA in TBST, WB  | Ab177952       |
| NHE3        | Biotrend   | Rabbit, polyclonal     | 1:200, 5% BSA in TBST, WB  | SPC-400D-A488  |
| PMCA        | ThermoFisher scientific                              | Mouse, monoclonal      | 1:1000, 5% BSA in TBST, WB | MA3-914        |
| Claudin 2   | ThermoFisher scientific                              | Mouse, monoclonal      | 1:1000, 5% BSA in TBST, WB | Ab2533085      |
| β Actin     | Sigma-Aldrich  | Mouse, monoclonal      | 1:2000, 5% BSA in TBST, WB | A2228          |
| NKCC2       | Kerim Mutig,<br>Charité – Universitätsmedizin Berlin | Guinea pig, polyclonal | 1:10 000 IF                | –              |

Abbreviations: AQP2, aquaporin 2; BSA, bovine serum albumin; IF, immunofluorescence; NCC, Na<sup>+</sup>-Cl<sup>−</sup> cotransporter; NCX1, Na<sup>+</sup>/Ca<sup>2+</sup> exchanger-1; NHE3, Na<sup>+</sup>/H<sup>+</sup> exchanger-3; NKCC2, Na<sup>+</sup>-K<sup>+</sup>-2Cl<sup>−</sup> cotransporter; PMCA, plasma membrane Ca<sup>2+</sup> ATPase; TBST, Tris-buffered saline with Tween20; TRPM6, transient receptor potential melastatin 6; TRPV5, luminal transient receptor potential cation channel subfamily V members 5; WB, western blotting.

## 4.5 | Statistical analysis

Pooled data are presented as mean ± SD. Statistical comparisons were performed using GraphPad Prism 9.1 for analysis of variance (ANOVA) followed by Tukey's multiple comparisons test. Comparative analysis between two groups was performed by unpaired *t* test. The threshold for statistical significance was set for *p* values <0.05.

## ACKNOWLEDGMENTS

This work was funded by the Deutsche Forschungsgemeinschaft (DFG, German Research Foundation)—project ID 394046635—SFB 1365. We thank Anette Drobbe for secretarial help, as well as Kerstin Riskowsky and Katja Dörfel for excellent technical assistance. Open Access funding enabled and organized by Projekt DEAL.

## FUNDING INFORMATION

Funded by the Deutsche Forschungsgemeinschaft (DFG, German Research Foundation)—project ID 394046635—SFB 1365.

## CONFLICT OF INTEREST

The authors declare no conflicts of interest.

## ORCID

Natalia Kriuchkova  <https://orcid.org/0000-0002-9795-2440>

Markus Bleich  <https://orcid.org/0000-0002-1745-2295>

Kerim Mutig  <https://orcid.org/0000-0001-9006-5112>

## REFERENCES

- Simon DB, Lu Y, Choate KA, et al. Paracellin-1, a renal tight junction protein required for paracellular Mg<sup>2+</sup> resorption. *Science*. 1999;285(5424):103-106.
- Konrad M, Schaller A, Seelow D, et al. Mutations in the tight-junction gene claudin 19 (CLDN19) are associated with renal magnesium wasting, renal failure, and severe ocular involvement. *Am J Hum Genet*. 2006;79(5):949-957.
- Shan Q, Himmerkus N, Hou J, Goodenough DA, Bleich M. Insights into driving forces and paracellular permeability from claudin-16 knockdown mouse. *Ann NY Acad Sci*. 2009;1165:148-151.
- Will C, Breiderhoff T, Thumfart J, et al. Targeted deletion of murine Cldn16 identifies extra- and intrarenal compensatory mechanisms of Ca<sup>2+</sup> and Mg<sup>2+</sup> wasting. *Am J Physiol Renal Physiol*. 2010;298(5):F1152-F1161.
- Hou J, Renigunta A, Gomes AS, et al. Claudin-16 and claudin-19 interaction is required for their assembly into tight junctions and for renal reabsorption of magnesium. *Proc Natl Acad Sci U S A*. 2009;106(36):15350-15355.
- Sikora P, Zaniew M, Haisch L, et al. Retrospective cohort study of familial hypomagnesaemia with hypercalciuria and nephrocalcinosis due to CLDN16 mutations. *Nephrol Dial Transplant*. 2015;30(4):636-644.
- Vall-Palomar M, Madariaga L, Ariceta G. Familial hypomagnesaemia with hypercalciuria and nephrocalcinosis. *Pediatr Nephrol*. 2021;36(10):3045-3055.
- Curry JN, Saurette M, Askari M, et al. Claudin-2 deficiency associates with hypercalciuria in mice and human kidney stone disease. *J Clin Invest*. 2020;130(4):1948-1960.
- Moor MB, Bonny O. Ways of calcium reabsorption in the kidney. *Am J Physiol Renal Physiol*. 2016;310(11):F1337-F1350.
- Milatz S, Himmerkus N, Wulfmeyer VC, et al. Mosaic expression of claudins in thick ascending limbs of Henle results in

- spatial separation of paracellular Na<sup>+</sup> and Mg<sup>2+</sup> transport. *Proc Natl Acad Sci U S A*. 2017;114(2):E219-E227.
11. Bleich M, Wulfmeyer VC, Himmerkus N, Milatz S. Heterogeneity of tight junctions in the thick ascending limb. *Ann NY Acad Sci*. 2017;1405(1):5-15.
  12. Gong Y, Renigunta V, Himmerkus N, et al. Claudin-14 regulates renal Ca<sup>2+</sup> transport in response to CaSR signalling via a novel microRNA pathway. *EMBO J*. 2012;31(8):1999-2012.
  13. van der Wijst J, van Goor MK, Schreuder MF, Hoenderop JG. TRPV5 in renal tubular calcium handling and its potential relevance for nephrolithiasis. *Kidney Int*. 2019;96(6):1283-1291.
  14. Staruschenko A. Regulation of transport in the connecting tubule and cortical collecting duct. In: Terjung R, ed. *Comprehensive Physiology*. Wiley; 2012:1541-1584.
  15. van Loon EPM, Little R, Prehar S, Bindels RJM, Cartwright EJ, Hoenderop JGJ. Calcium extrusion pump PMCA4: a new player in renal calcium handling? *PLoS ONE*. 2016;11(4):e0153483.
  16. Ellison DH, Maeoka Y, McCormick JA. Molecular mechanisms of renal magnesium reabsorption. *J Am Soc Nephrol*. 2021;32(9):2125-2136.
  17. Curry JN, Yu ASL. Magnesium handling in the kidney. *Adv Chronic Kidney Dis*. 2018;25(3):236-243.
  18. Mount DB. Thick ascending limb of the loop of Henle. *Clin J Am Soc Nephrol*. 2014;9(11):1974-1986.
  19. Günzel D, Yu ASL. Function and regulation of claudins in the thick ascending limb of Henle. *Pflugers Arch - Eur J Physiol*. 2009;458(1):77-88.
  20. Breiderhoff T, Himmerkus N, Drewell H, et al. Deletion of claudin-10 rescues claudin-16-deficient mice from hypomagnesemia and hypercalciuria. *Kidney Int*. 2018;93(3):580-588.
  21. Muto S, Hata M, Taniguchi J, et al. Claudin-2-deficient mice are defective in the leaky and cation-selective paracellular permeability properties of renal proximal tubules. *Proc Natl Acad Sci U S A*. 2010;107(17):8011-8016.
  22. Pan W, Borovac J, Spicer Z, et al. The epithelial sodium/proton exchanger, NHE3, is necessary for renal and intestinal calcium (re)absorption. *Am J Physiol Renal Physiol*. 2012;302(8):F943-F956.
  23. Raja KA. Responsiveness of hypercalciuria to thiazide in Dent's disease. *J Am Soc Nephrol*. 2002;13(12):2938-2944.
  24. Nijenhuis T, Vallon V, van der Kemp AWC, Loffing J, Hoenderop JGJ, Bindels RJM. Enhanced passive Ca<sup>2+</sup> reabsorption and reduced Mg<sup>2+</sup> channel abundance explains thiazide-induced hypocalciuria and hypomagnesemia. *J Clin Invest*. 2005;115(6):1651-1658.
  25. Bergsland KJ, Worcester EM, Coe FL. Role of proximal tubule in the hypocalciuric response to thiazide of patients with idiopathic hypercalciuria. *Am J Physiol Renal Physiol*. 2013;305(4):F592-F599.
  26. Gesek FA, Friedman PA. Mechanism of calcium transport stimulated by chlorothiazide in mouse distal convoluted tubule cells. *J Clin Invest*. 1992;90(2):429-438.
  27. Yu X, Duan K-L, Shang C-F, Yu H-G, Zhou Z. Calcium influx through hyperpolarization-activated cation channels (I<sub>h</sub>) channels contributes to activity-evoked neuronal secretion. *Proc Natl Acad Sci U S A*. 2004;101(4):1051-1056.
  28. Loffing J, Loffing-Cueni D, Hegyi I, et al. Thiazide treatment of rats provokes apoptosis in distal tubule cells. *Kidney Int*. 1996;50(4):1180-1190.
  29. Nijenhuis T, Hoenderop JGJ, Loffing J, van der Kemp AWC, van Os CH, Bindels RJM. Thiazide-induced hypocalciuria is accompanied by a decreased expression of Ca<sup>2+</sup> transport proteins in kidney. *Kidney Int*. 2003;64(2):555-564.
  30. Loffing J. Altered renal distal tubule structure and renal Na<sup>+</sup> and Ca<sup>2+</sup> handling in a mouse model for Gitelman's syndrome. *J Am Soc Nephrol*. 2004;15(9):2276-2288.
  31. Maeoka Y, McCormick JA. NaCl cotransporter activity and Mg<sup>2+</sup> handling by the distal convoluted tubule. *Am J Physiol Renal Physiol*. 2020;319(6):F1043-F1053.
  32. Alexander RT, Dimke H. Effect of diuretics on renal tubular transport of calcium and magnesium. *Am J Physiol Renal Physiol*. 2017;312(6):F998-F1015.
  33. Beggs MR, Young K, Pan W, et al. Claudin-2 and claudin-12 form independent, complementary pores required to maintain calcium homeostasis. *Proc Natl Acad Sci U S A*. 2021;118(48):e2111247118.
  34. Alexander RT, Dimke H. Molecular mechanisms underlying paracellular calcium and magnesium reabsorption in the proximal tubule and thick ascending limb. *Ann NY Acad Sci*. 2022;1518:69-83.
  35. Plain A, Pan W, O'Neill D, et al. Claudin-12 knockout mice demonstrate reduced proximal tubule calcium permeability. *Int J Mol Sci*. 2020;21(6):2074.
  36. Himmerkus N, Shan Q, Goerke B, Hou J, Goodenough DA, Bleich M. Salt and acid-base metabolism in claudin-16 knockdown mice: impact for the pathophysiology of FHHNC patients. *Am J Physiol Renal Physiol*. 2008;295(6):F1641-F1647.
  37. Alexander RT, Dimke H, Cordat E. Proximal tubular NHEs: sodium, protons and calcium? *Am J Physiol Renal Physiol*. 2013;305(3):F229-F236.
  38. Eisner C, Faulhaber-Walter R, Wang Y, et al. Major contribution of tubular secretion to creatinine clearance in mice. *Kidney Int*. 2010;77(6):519-526.
  39. Tucker BJ, Blantz RC. Effect of furosemide administration on glomerular and tubular dynamics in the rat. *Kidney Int*. 1984;26(2):112-121.
  40. Loffing J, Loffing-Cueni D, Valderrabano V, et al. Distribution of transcellular calcium and sodium transport pathways along mouse distal nephron. *Am J Physiol Renal Physiol*. 2001;281(6):F1021-F1027.
  41. Hoenderop JGJ, van Leeuwen JPTM, van der Eerden BCJ, et al. Renal Ca<sup>2+</sup> wasting, hyperabsorption, and reduced bone thickness in mice lacking TRPV5. *J Clin Invest*. 2003;112(12):1906-1914.
  42. Grimm PR, Lazo-Fernandez Y, Delpire E, et al. Integrated compensatory network is activated in the absence of NCC phosphorylation. *J Clin Invest*. 2015;125(5):2136-2150.
  43. Grimm PR, Coleman R, Delpire E, Welling PA. Constitutively active SPAK causes hyperkalemia by activating NCC and remodeling distal tubules. *J Am Soc Nephrol*. 2017;28(9):2597-2606.
  44. Saritas T, Puelles VG, Su X-T, McCormick JA, Welling PA, Ellison DH. Optical clearing in the kidney reveals potassium-mediated tubule remodeling. *Cell Rep*. 2018;25(10):2668-2675.e3.
  45. Câmpăan V, Kricke J, Ellison D, Luft FC, Bachmann S. Localization of thiazide-sensitive Na(+)-Cl(-) cotransport and associated gene products in mouse DCT. *Am J Physiol Renal Physiol*. 2001;281(6):F1028-F1035.
  46. Hofmeister MV, Fenton RA, Praetorius J. Fluorescence isolation of mouse late distal convoluted tubules and connecting

- tubules: effects of vasopressin and vitamin D3 on  $\text{Ca}^{2+}$  signaling. *Am J Physiol Renal Physiol*. 2009;296(1):F194-F203.
47. de Groot T, Lee K, Langeslag M, et al. Parathyroid hormone activates TRPV5 via PKA-dependent phosphorylation. *J Am Soc Nephrol*. 2009;20(8):1693-1704.
48. Lee M, Partridge NC. Parathyroid hormone signaling in bone and kidney. *Curr Opin Nephrol Hypertens*. 2009;18(4):298-302.
49. Fluck EC, Yazici AT, Rohacs T, Moiseenkova-Bell VY. Structural basis of TRPV5 regulation by physiological and pathophysiological modulators. *Cell Rep*. 2022;39(4):110737.
50. de Bruijn PIA, Larsen CK, Frische S, et al. Furosemide-induced urinary acidification is caused by pronounced  $\text{H}^+$  secretion in the thick ascending limb. *Am J Physiol Renal Physiol*. 2015;309(2):F146-F153.
51. Saritas T, Borschewski A, McCormick JA, et al. SPAK differentially mediates vasopressin effects on sodium cotransporters. *J Am Soc Nephrol*. 2013;24(3):407-418.

## SUPPORTING INFORMATION

Additional supporting information can be found online in the Supporting Information section at the end of this article.

**How to cite this article:** Kriuchkova N, Breiderhoff T, Müller D, et al. Furosemide rescues hypercalciuria in familial hypomagnesaemia with hypercalciuria and nephrocalcinosis model. *Acta Physiol*. 2023;237:e13927. doi:[10.1111/apha.13927](https://doi.org/10.1111/apha.13927)